



HAL
open science

Graphitization and amorphization of textured carbon using high-energy nanosecond laser pulses

Loïc Loisel, Marc Châtelet, Guillaume Giudicelli, Mathias Lebihain, Yi Yang,
Costel-Sorin Cojocaru, Andrei Constantinescu, Beng Kang Tay, Bérengère
Lebental

► **To cite this version:**

Loïc Loisel, Marc Châtelet, Guillaume Giudicelli, Mathias Lebihain, Yi Yang, et al.. Graphitization and amorphization of textured carbon using high-energy nanosecond laser pulses. *Carbon*, 2016, 105, pp.227-232. 10.1016/j.carbon.2016.04.026 . hal-01765284

HAL Id: hal-01765284

<https://hal.science/hal-01765284v1>

Submitted on 18 Feb 2020

HAL is a multi-disciplinary open access archive for the deposit and dissemination of scientific research documents, whether they are published or not. The documents may come from teaching and research institutions in France or abroad, or from public or private research centers.

L'archive ouverte pluridisciplinaire **HAL**, est destinée au dépôt et à la diffusion de documents scientifiques de niveau recherche, publiés ou non, émanant des établissements d'enseignement et de recherche français ou étrangers, des laboratoires publics ou privés.



Distributed under a Creative Commons Attribution 4.0 International License

Graphitization and amorphization of textured carbon using high-energy nanosecond laser pulses

Loïc Loisel ^{a, b, c, *}, Marc Châtelet ^c, Guillaume Giudicelli ^d, Mathias Lebihain ^d, Yi Yang ^e, Costel-Sorin Cojocaru ^c, Andrei Constantinescu ^d, Beng Kang Tay ^{a, b}, Bérengère Lebental ^{c, f}

^a CINTRA CNRS/NTU/Thalès, UMI 3288, 50 Nanyang Drive, Singapore

^b School of Electrical and Electronics Engineering, Nanyang Technological University, 50 Nanyang Avenue, Singapore

^c LPICM, CNRS, Ecole Polytechnique, Université Paris Saclay, 91128, Palaiseau, France

^d LMS, Ecole Polytechnique, CNRS, Université Paris-Saclay, 91128, Palaiseau, France

^e Data Storage Institute, A*STAR, 5 Engineering Drive 1, Singapore

^f Université Paris-Est, IFSITAR, 14-20 Bd Newton, Champs-sur-Marne, Marne-la-Vallée, France

Laser pulses can effectively induce local structural changes and modify the physical properties of carbon allotropes. So far, only graphitization has been demonstrated using low laser energies ($\leq 1 \text{ J} / \text{cm}^2$). The novelty of this paper is a result of laser-induced amorphization of a highly anisotropic carbon allotrope by using high energy ($1.5\text{--}15.4 \text{ J/cm}^2$) 5 ns, 532 nm Nd-YAG laser pulses. Moreover, cycling phase change, between an amorphous and a crystalline phase, is also obtained by adjusting the pulse energy. However, cycling ability is restricted to a few cycles as a consequence of laser-induced surface damages caused by both high temperatures during and high thermal gradients during and after laser exposure. The occurrence of graphitization or amorphization depends on the amount of solid crystalline seeds during so-lidification from the melt, which is controlled by the post-pulse temperature of the carbon surface. This study uncovers new applications of carbon allotropes, such as optically-controlled reversible phase-change memories.

1. Introduction

Carbon allotropes are key building blocks in a wide range of applications as they feature extremely versatile electrical, mechanical and optical properties. This versatility is linked to the variability in their crystalline structure, in particular the sp^2 (graphite-like) to sp^3 (diamond-like) atomic bond ratio or the amounts of sp^2 clustering and of disorder [1,2].

As a result, numerous research groups have proposed different methods to control the atomic structure of carbon allotropes. Partial control of the atomic structure of carbon thin films can be achieved during deposition by tuning the deposition parameters [3–7] or after deposition by slow thermal annealing in an oven [8–13]. In a more localized manner and to induce rapid changes,

beams of electrons [14], ions [15], or photons [16–20] can be used. However, only the application of an electric field in electronic devices has enabled reversible changes, through the formation and rupture of graphitic filaments [21–25]. This has opened the way toward electrically-controlled carbon-based resistive memories [21,24,25].

The continuous development of optical technologies such as the widespread Blu-Ray technique has demonstrated that using photons instead of an electric-field to induce reversible phase changes is of both technological and commercial interest [26].

So far, laser-based phase change experiments have only conducted to graphitization and not to amorphization, hence obstructing further device applications, including optical memories. However, most studies have focused exclusively on a small energy density window, below 1 J/cm^2 , to avoid surface degradations [16–18,20]. As a consequence, surface damages on carbon films have been mostly overlooked, despite their critical impact on applications ranging from crystallization to ablation.

* Corresponding author. LPICM, CNRS, Ecole Polytechnique, Université Paris Saclay, 91128, Palaiseau, France.

E-mail address: loic.loisel@polytechnique.edu (L. Loisel).

The goal of this paper is to demonstrate optically-induced reversible phase change in carbon. Here, we present a detailed study on the impact of high-energy laser pulses (1.5–15.4 J/cm²) on the crystalline content and surface morphology of two films of textured carbon. This material consists of nano-sized clusters of graphitic planes that are preferentially oriented perpendicular to the substrate, therefore it has attracted a large interest for applications in electronics and thermal management [14,16,17,27–29]. Moreover, as the crystalline regions are separated by amorphous carbon, textured carbon is neither fully amorphous nor fully crystalline, consequently it is highly suitable for the investigation of laser-induced crystallization or amorphization.

We show that laser-induced amorphization of carbon is possible, *i.e.* the phase change from crystalline to amorphous, can be obtained for sufficiently high energy laser pulses. The reversible phase change can be explained by considering crystallization kinetics and the impact of solid crystallization seeds. This demonstration of reversibility makes the development of phase-change memories feasible: we provide a proof of concept by studying the cycling ability of textured carbon phase change. Critically for carbon laser-annealing applications, we also study the resulting surface state by classifying the surface damages. We show that different surface artefacts appear for different thermal gradients and temperatures.

2. Experimental details

2.1. Preparation of the films

Two thin films of textured carbon [27] are deposited by a Filtered Cathodic Vacuum Arc [30] system on two separate Si substrates for the annealing experiments. The deposition parameters are a bias voltage of –500 V on the substrate, an arc current of 60 A and a pressure in the chamber of $4 \cdot 10^{-6}$ Torr before deposition and a maximum of 10^{-5} Torr during deposition. The deposition duration is 9 min for one substrate, 2 min for the second. Using a Dektak XT surface profiler, the two films are found to be respectively 310 ± 120 nm and 110 ± 40 nm thick. We refer to them as “sample A” and “sample B”, respectively.

2.2. Laser-annealing

Annealing is conducted in ambient atmosphere with a 532 nm Surelite I-10 Nd-YAG laser, with energy tunable between 110 and 900 mJ, emitting single 5 ns pulses. Before annealing, the total pulse energy and the non-uniform spatial distribution of the pulses are characterized with a Labmax_Top power metre and an Ophir M2-200s beam profiler (see Supplementary Material Section 1). The samples are mounted on a mobile stage normally to the beam at approximately 300 mm from the source and annealed by single pulses. After each pulse, the film is translated normally to the beam by 6 mm to prevent overlap between neighbouring annealed areas. In total, 41 pulses are shot on sample A and 24 on sample B.

2.3. Post-annealing characterization

After laser exposure, the surface morphology of the films is observed with a LEO 1550 Gemini Field Emission SEM.

Bright-field and high-resolution TEM analysis are performed by a FEI Titan TEM at 300 kV. TEM samples are prepared by using a Focused Ion Beam Helios 450 S, at 30 kV for coarse milling, and at 5 kV for final fine milling (to reduce surface amorphization effects by the high-energy Ga ions used in FIB sample preparation).

To characterize the atomic structure quantitatively and non-destructively, Raman spectroscopy is carried out with a WITec

532 nm Raman microscope. The laser is used at low intensity to prevent annealing during characterization [19]. Unless stated otherwise, Raman spectra are acquired roughly at the energetic centre of each annealed spot. Broad G (1580 cm⁻¹), D (1350 cm⁻¹) and T (1060 cm⁻¹) bands are observed. To extract the desired data from the spectra, we use an automated parameter extraction method based on Lorentzian fit (Supplementary Material, Section 2). Moreover, a Bootstrap method [31] is applied to derive the uncertainty range for the extracted Raman parameters, which reaches around 4% on the I(D)/I(G) ratio. The extracted Raman parameter values are interpreted according to the standing framework for strongly disordered graphite, semi-crystalline carbon and amorphous carbon [1,32]: the G peak is associated to bond stretching of sp² pairs, while the D band is associated with defective rings of sp² atoms. The T band, more commonly monitored with UV Raman spectroscopy [1] but observed in the spectra acquired here, indicates the presence of atoms in sp³ configuration. The spatial variability in the Raman spectra (*e.g.* due to the position of the beam with respect to the sample) is assessed on the pristine film and found to be much smaller than the observed variations due to laser-annealing (Supplementary Material, Section 3).

3. Results and discussion

3.1. Reversible phase change

As-deposited textured carbon is composed of clusters of graphitic planes perpendicular to the substrate and separated by amorphous regions, as shown by the HRTEM images (Fig. 1 (a)) and the electron diffraction pattern showing the (002) reflection peaks of graphite (Fig. 1 (a) inset).

The Raman spectrum of pristine textured carbon (Fig. 2 (a), *inset*, bottom spectrum, “as-deposited”) yields the following parameters: I(D)/I(G) = 0.69 ± 0.01 ; G peak position $x_G = 1548 \pm 1$ cm⁻¹; full width at half maximum (FWHM) of the G peak $w_G = 268 \pm 3$ cm⁻¹. These values are consistent with a mostly sp² carbon allotrope with up to 20% of sp³ atoms [32].

After laser annealing with increasing energy densities, we observe in both films a continuous increase of the D peak intensity (Fig. 2 (a)) while the width of both the D and G peaks decreases (see Supplementary Material, Section 4). In sample A (respectively sample B), the maximum I(D)/I(G) is reached at 4.3 J/cm² (respectively 2.0 J/cm²), corresponding to a 43% (respectively 15%) increase from the pristine material. These results are consistent with carbon graphitization. Similar graphitization trends have been reported at energy densities below 1 J/cm² [16–19]. HRTEM images of sample A annealed at 4.3 J/cm² show that the structure of laser-annealed textured carbon is composed mainly of graphitic planes (Fig. 1 (b)) that are found to remain mostly perpendicular to the substrate (similarly to the pristine material).

Then, from 4.3 J/cm² upward (respectively from 2.0 J/cm²), the I(D)/I(G) ratio decreases continuously and the peaks broaden. It indicates a continuous evolution from a graphite-like material to a more amorphous carbon. At about 10 J/cm² (respectively 4.3 J/cm²), I(D)/I(G) values reach their initial level (their level in the pristine material). Beyond 10 J/cm² (respectively 4.3 J/cm²), the amorphization trend continues (Fig. 2 (a)): I(D)/I(G) decreases down to –65% (respectively –64%) from the pristine material.

Fig. 1 (c) and (d) are HRTEM cross-sections of sample A after laser annealing with a 14.2 J/cm² pulse. Supporting the Raman data, it is found that most of the carbon layer has become amorphous, except at the C/Si interface where graphitic planes following the Si–C interface are observed (Fig. 1 (d)). The Si layer also appears to be degraded. Though no SiC Raman peaks (at *ca.* 760 and 960 cm⁻¹) are detected, the presence of SiC at the Si–C interface may not be

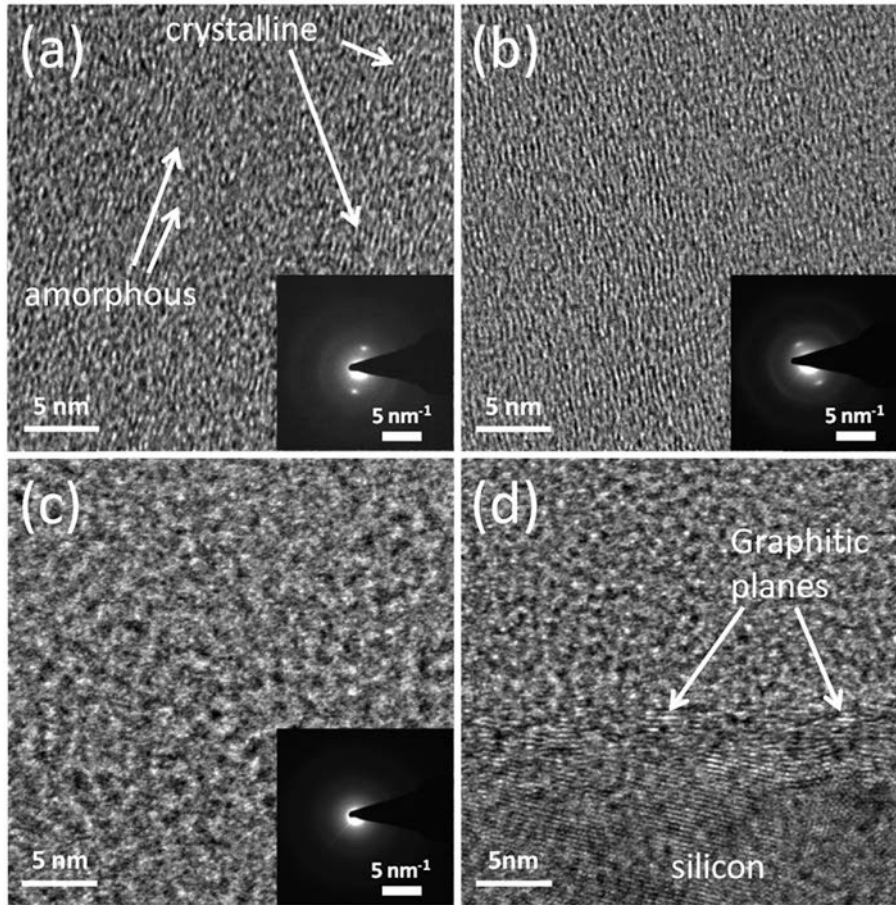


Fig. 1. Cross-section HRTEM images of sample A: (a) pristine area showing the vertical graphitic planes of un-annealed textured carbon (inset: diffraction pattern), (b) cross-section of the material after annealing at 4.3 J/cm^2 showing the more crystalline material, with graphitic planes perpendicular to the substrate (inset: diffraction pattern), (c) cross-section of the material after annealing at 14.2 J/cm^2 showing amorphized carbon (inset: diffraction pattern), (d) cross-section of the material after annealing at 14.2 J/cm^2 showing graphitic planes parallel to the Si/C interface.

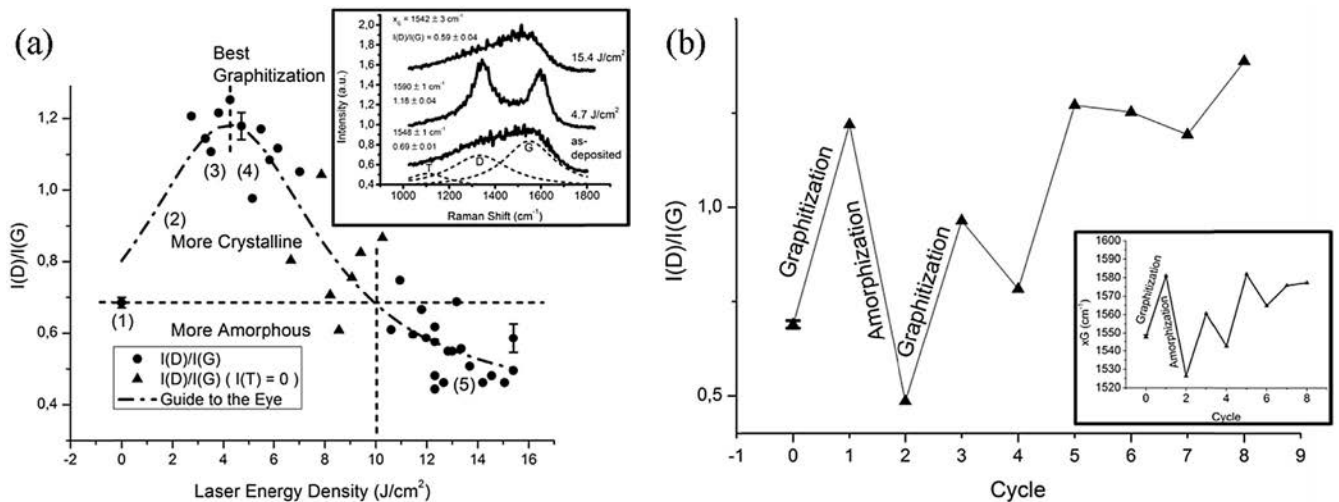


Fig. 2. (a) $I(D)/I(G)$ as a function of the energy density after laser-annealing of sample A. *Inset:* Raman spectra for three different energy densities. (b) Study of the cycling ability: $I(D)/I(G)$ values after laser-annealing with alternating graphitizing (3.8 J/cm^2 ; Cycles 1, 3, 5, 7) and amorphizing (12.3 J/cm^2 ; Cycles 2, 4, 6, 8) pulses (sample A). Cycle 0 corresponds to the pristine material.

excluded, as SiC vibrations have a very small cross-section [1].
By looking at the Raman data on the whole range of energies, it is found that the threshold energies (for graphitization and

amorphization) and maximum $I(D)/I(G)$ values are higher in the thicker sample A than in the thinner sample B (Supplementary Material, Section 5). This suggests that volume mechanisms are

involved in the phase change.

Overall the data show that, depending on their energy density, nanosecond laser pulses can trigger either graphitization or amorphization in textured carbon thin films. While laser-induced graphitization of carbon has been reported several times, it is the first time laser-induced amorphization is achieved. The phase change is reversible, as demonstrated when annealing the same spot with alternating high and low energy pulses (Fig. 2 (b)). However, the cycling ability is low (3 cycles), hinting at irreversible degradations in the material during laser exposure. To understand the origins of this irreversibility, we carry out an analysis of the surface morphology of the laser-annealed regions.

3.2. Laser-induced damages

Previous studies on low energy laser-annealing of amorphous carbon (a-C) report a slight increase in surface roughness [17]. Here, SEM images confirm this trend for pulses between 1.5 J/cm^2 and 3.9 J/cm^2 (for sample A). The increase in roughness is due to spherical surface grains, whose density and size increase with increasing pulse energy (Fig. 3, (a) and (b)). In the literature, such grains are attributed to localized melting of the top carbon layer during annealing, followed by air-cooling and rapid solidification [33]. This suggests that the surface of the textured carbon layer reaches its melting temperature at energy densities as low as 1.5 J/cm^2 . Let us remark that the melting temperature of textured carbon has never been measured. However, as it is composed of a mixture of sp^2 and sp^3 bonded atoms [27] with similar cohesive energies [34], the melting temperature of textured carbon is expected to be close to that of graphite (4450 K [35]). Laser-induced melting of graphite has been reported at energy densities as low as 0.6 J/cm^2 [33,36–40].

To support the hypothesis that the film partially melts at energy densities as low as 1.5 J/cm^2 , we study by numerical modelling the temperature rise in a vertical graphitic film, that is, where the graphitic planes are aligned perpendicularly to the substrate similar to textured carbon. The material is annealed by a 5 ns energetic laser pulse. We use the finite element method with the software Cast3M [41]. We find that at energy densities as low as 0.6 J/cm^2 , the surface temperature rises above the melting temperature (while most of the film remains at temperatures lower

than the melting temperature). A detailed discussion of these results is provided in the Supplementary Material, Section 6.

In a small range of energies around 3.9 J/cm^2 , cracks (Fig. 3 (c) and (d)) are observed. They uncover the Si layer locally, so that at crack locations, only Si Raman peaks can be observed. Cracks are known features of nanosecond laser annealing experiments [33] caused by strong thermal gradients in the solid phase. The occurrence of cracks at 3.9 J/cm^2 thus indicates that at such energy densities, the carbon film is still partially solid and undergoes thermal gradients reaching throughout the layer. The absence of cracks below this threshold suggests that the large thermal gradients remain confined to the surface. The renewed absence of cracks above this threshold suggests that the carbon film is then fully melted. The small energy window for crack appearance can be explained by the high thermal conductivity of liquid carbon (nearly 10 times larger than solid carbon [36]), which fosters the downward diffusion of the heat toward the solid/liquid interface and the fusion of the solid layer. In other words, when the film starts melting homogeneously, full melting occurs very rapidly. Similar processes have been reported during laser-annealing of Si [42]. Interestingly, in the thinner sample only (B) and in the direct vicinity of the cracks, wave-like structures with a roughly 500 nm period are observed (Fig. 3 (d)). Such ripples are common features in laser-annealed crystalline Si films. Appearing when the Si surface temperature is close to its melting point [43], they are attributed to light-induced electronic surface waves (plasmons) and have a period equal to the excitation wavelength when the light direction is normal to the surface [44].

However, ripples have never been reported after laser-annealing of disordered carbon; moreover, at 3.9 J/cm^2 , the carbon layer surface is thought to be significantly above its melting temperature. Consequently, we postulate that the ripples do not appear directly in the C layer, but rather appear in the Si layer around the locations where it is uncovered by the cracked C layer; upon cooling, the carbon melt solidifies around Si ripples, forming the structures observed here. They are not apparent in the thick film as the layer thickness is much larger than the ripple height. This interpretation further entails that at 3.9 J/cm^2 , the Si/C interface temperature is close to the Si melting point (1680 K), while the top carbon layer temperature is above its melting point (4450 K).

When the energy density increases above the cracking

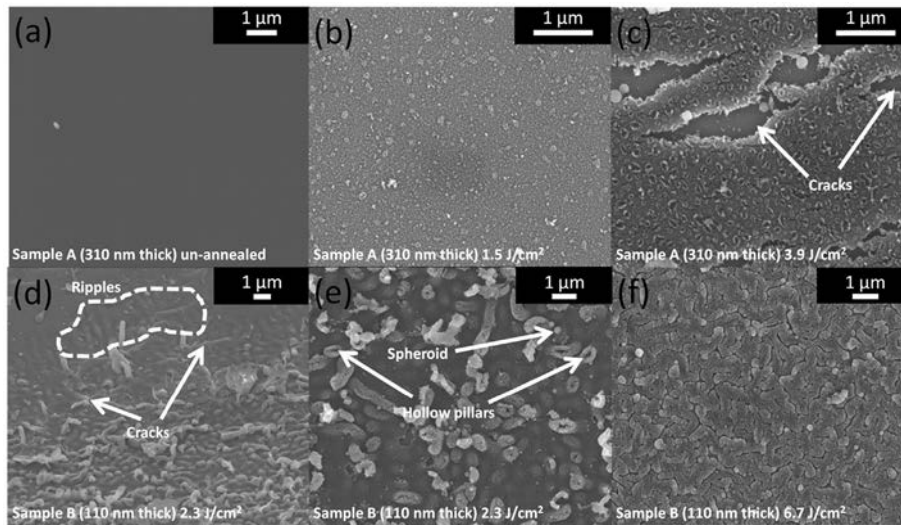


Fig. 3. Features commonly observed at the surface of un-annealed and laser-annealed textured carbon. (a) Smooth un-annealed surface. (b) Increasing surface roughness at low energy densities. (c) Appearance of cracks. (d) Cracks and ripples that are observed only on the surface of Sample B. (e) Sputtering traces (spheroids and hollow pillars). (f) Explosive boiling traces.

threshold, from 3.9 to 6 J/cm² (sample A), the size and density of the surface grains increase (Fig. 3 (c)). Grain shapes evolve progressively from spherical to anisotropic, yielding full or hollow cylinders (pillars or tubes). The tubes and pillars are attributed to the sudden quenching of the carbon layer at the end of the laser pulse. The different structures (full or hollow cylinders) suggest that the carbon layer boils during the pulse and that bubbles of liquid carbon are frozen at different stages of their vaporization. The hollow cylinders (whose number increases with increasing energy) indicate that some sputtering takes place. This conforms with the literature, which indicates that sputtering occurs when the temperature increases significantly above the melting point [33].

Finally, at even higher energy densities, between 6 and 15.4 J/cm², the surface microstructure shows important matter restructuration, forming deep grooves and ridges. Signs of secondary sputtering (spheroids on the remaining material) are also observed (Fig. 3 (f) for this observation on Sample B). We recall that surface boiling is attained at energy densities as low as 3.9 J/cm², so in this energy range, the surface temperature of the carbon layer is expected to be far above its boiling point. We attribute the matter restructuration to explosive boiling, the main mechanism used in laser ablation techniques [45,46]. Estimates of temperatures required for explosive boiling of graphite vary drastically, between 6710 K and 22,400 K [46]. The secondary sputtering phase is thought to occur right after explosive boiling and during cooling, when the remaining material returns to boiling temperature. Similar boiling processes have been reported in Si [47].

3.3. Mechanisms controlling the reversible phase change

Table 1 summarizes the results in terms of crystallinity, surface and volume states of the annealed spots for sample A. We now exploit this table to propose an interpretation of the crystallization mechanism.

First of all, as the annealing is conducted in air, it is important to discuss the possibility that oxygen plays a role in the observed phase and morphology changes. Our numerical model (Supplementary Material section 6) and other results in the literature [36] show that during nanosecond laser annealing, the temperature rises above the melting point and decreases back to temperatures close to room temperature in much less than 1 μs. By comparison, carbon oxidation is known to occur at a timescale in the range of minutes [48], so its impact is expected to be negligible within 1 μs. This fact is supported by EELS maps of the oxygen content obtained on cross-sections of the un-annealed film and the film annealed with a 4.3 and a 14.2 J/cm² laser pulse. These cross-sections (see Supplementary Material Section 7) show that after annealing with medium (4.3 J/cm²) or high (14.2 J/cm²) energy densities, there is no

visible increase in the oxygen content of the films.

Since oxidation plays no role in the phase change and surface damages, these phenomena should be explained considering mechanisms of extremely rapid thermal annealing and cooling; similar mechanisms are at stake in phase change memory devices [49] and in the manufacturing of glassy materials (quenching from the liquid state).

In sample A, at energy densities up to 3.9 J/cm², the melting of the C layer is partial, so solid carbon growth seeds are present during solidification. These seeds are expected to be more crystalline than the pristine material, because the amorphous carbon component of textured carbon is expected to melt first, its cohesive energy being smaller than that of crystalline carbon [34,50]. A more crystalline material is obtained from these more crystalline seeds [51].

At slightly higher energy densities, even when the carbon layer is fully molten, the Si layer may still act as a growth seed, as evidenced by the epitaxial growth observed in TEM images at the Si/C interfaces (Fig. 1 (d)).

At much higher energy densities, the molten Si front moves much further away from the carbon interface into the Si substrate. Conjointly, the time spent in the melt is longer [36], which tends to reduce the thermal gradients during cooling, which in turns yields a more homogeneous solidification. As a consequence, the carbon melt solidifies without contact to any crystalline growth boundary, which results in a strongly amorphous material. This amorphization process contrasts with fast cooling processes in that what matters most is not the cooling speed but rather that the solidification occurs in the absence of crystallization catalysts.

4. Conclusion

The results are foremost a proof of laser-induced amorphization of a carbon film, achieved using high energy density pulses. The outcome is a first critical step for the development of laser-controlled carbon phase change memories. Moreover, it is a further proof for laser-induced graphitization, which is consistent with prior results in the literature. The proposed method permits to obtain both phases and to study the cyclic phase change. However the actual conditions allow only limited cycling as a consequence of a weak endurance. A detailed surface study reveals significant matter loss resulting from the intense thermal gradients and high temperatures occurring during annealing. The spatial thermal gradients at crystallization temperatures, during the solidification of the melt, have been revealed as the main differentiation factor between graphitization (heterogeneous solidification, strong gradients) and amorphization (homogeneous solidification, small gradients).

Table 1

Qualitative description of the crystallinity, surface state and molten state for sample A. Graphitization and Amorphization mean respectively increasing and decreasing quantity of sp² crystals.

Energy range	1.5 J/cm ² to 3.9 J/cm ²		3.9 J/cm ² to 6 J/cm ²	6 J/cm ² to 10 J/cm ²	10 J/cm ² to 15.4 J/cm ²
Crystallinity Compared to Pristine	Graphitization	Best Graphitization	Amorphization	Amorphization	Amorphization Threshold
Surface State	Spheroids on smooth layer. Localized melting	Cracks; ripples (sample B only). Partial surface covering with spheroid, pillars and tubes at boiling temperature	Spheroids, pillars and tubes covering the whole surface. Surface above boiling temperature	Grooves and ridges with secondary sputtering. Loss of matter due to explosive boiling	
Volume Effect	Solid C and Si film	Partially Molten C film, solid Si film; Cracking and Delamination	Fully Molten C film; Partially Molten Si film	Molten C film at temperature far above boiling temperature Partially molten Si film	

Acknowledgements

We thank Dr. Li Xiaohui (NTU) for his assistance in handling the beam profiler and obtaining beam profile images. Loïc Loisel is grateful for having been awarded the SINGA scholarship, without which he would not have been able to be involved in this research. We thank Dr. Liu Binghai (Global Foundries) for his assistance in the HRTEM experiments, and for useful discussions about the preparation of TEM lamellae.

References

- [1] A.C. Ferrari, J. Robertson, Raman spectroscopy of amorphous, nanostructured, diamond like carbon, and nanodiamond, *Philos. Trans. R. Soc. Lond. Ser. A* 362 (1824) (2004) 2477–2512.
- [2] J. Robertson, Diamond-like amorphous carbon, *Mater. Sci. Eng. R Rep.* 37 (4–6) (2002) 129–281.
- [3] D. Lau, D. McCulloch, M. Taylor, J. Partridge, D. McKenzie, N. Marks, et al., Abrupt stress induced transformation in amorphous carbon films with a highly conductive transition phase, *Phys. Rev. Lett.* 100 (17) (2008) 176101.
- [4] A.A. Voevodin, M.S. Donley, Preparation of amorphous diamond-like carbon by pulsed laser deposition: a critical review, *Surf. Coat. Technol.* 82 (3) (1996) 199–213.
- [5] T.A. Friedmann, K.F. McCarty, J.C. Barbour, M.P. Siegal, D.C. Dibble, Thermal stability of amorphous carbon films grown by pulsed laser deposition, *Appl. Phys. Lett.* 68 (12) (1996) 1643–1645.
- [6] D.R. McKenzie, D. Muller, B.A. Pailthorpe, Compressive-stress-induced formation of thin-film tetrahedral amorphous carbon, *Phys. Rev. Lett.* 67 (6) (1991) 773–776.
- [7] M. Chhowalla, A.C. Ferrari, J. Robertson, G.A.J. Amarantunga, Evolution of sp² bonding with deposition temperature in tetrahedral amorphous carbon studied by Raman spectroscopy, *Appl. Phys. Lett.* 76 (11) (2000) 1419–1421.
- [8] A.C. Ferrari, B. Kleinsorge, N.A. Morrison, A. Hart, V. Stolojan, J. Robertson, Stress reduction and bond stability during thermal annealing of tetrahedral amorphous carbon, *J. Appl. Phys.* 85 (10) (1999) 7191–7197.
- [9] J.O. Orwa, I. Andrienko, J.L. Peng, S. Praver, Y.B. Zhang, S.P. Lau, Thermally induced sp² clustering in tetrahedral amorphous carbon (taC) films, *J. Appl. Phys.* 96 (11) (2004) 6286–6297.
- [10] A. Ilić, A.C. Ferrari, T. Yagi, J. Robertson, Effect of sp²-phase nanostructure on field emission from amorphous carbons, *Appl. Phys. Lett.* 76 (18) (2000) 2627–2629.
- [11] N.M.J. Conway, A.C. Ferrari, A.J. Flewitt, J. Robertson, W.I. Milne, A. Tagliaferro, et al., Defect and disorder reduction by annealing in hydrogenated tetrahedral amorphous carbon, *Diam. Relat. Mater.* 9 (3 6) (2000) 765–770.
- [12] K. Takai, M. Oga, H. Sato, T. Enoki, Y. Ohki, A. Taomoto, et al., Structure and electronic properties of a nongraphitic disordered carbon system and its heat-treatment effects, *Phys. Rev. B Condens. Matter* 67 (21) (2003) 214202.
- [13] D.G. McCulloch, J.L. Peng, D.R. McKenzie, S.P. Lau, D. Sheeja, B.K. Tay, Mechanisms for the behavior of carbon films during annealing, *Phys. Rev. B Condens. Matter* 70 (8) (2004) 085406.
- [14] E. Teo, A. Bolker, R. Kalish, C. Saguy, Nano-patterning of through-film conductivity in anisotropic amorphous carbon induced using conductive atomic force microscopy, *Carbon* 49 (8) (2011) 2679–2682.
- [15] L.A. Farrow, B.J. Wilkens, A.S. Gozdz, D.L. Hart, Raman scattering and hydrogen-content analysis of amorphous hydrogenated carbon films irradiated with 200-keV C⁺ ions, *Phys. Rev. B* 41 (14) (1990) 10132–10137.
- [16] M. Shakerzadeh, N. Xu, M. Bosman, B. Tay, X. Wang, E. Teo, et al., Field emission enhancement and microstructural changes of carbon films by single pulse laser irradiation, *Carbon* 49 (3) (2011) 1018–1024.
- [17] N. Xu, H.T.E. Teo, M. Shakerzadeh, X. Wang, C.M. Ng, B.K. Tay, Electrical properties of textured carbon film formed by pulsed laser annealing, *Diam. Relat. Mater.* 23 (2012) 135–139.
- [18] Y. Miyajima, A.A.D.T. Adikaari, S.J. Henley, J.M. Shannon, S.R.P. Silva, Electrical properties of pulsed UV laser irradiated amorphous carbon, *Appl. Phys. Lett.* 92 (15) (2008) 152104–152113.
- [19] M. Bowden, D.J. Gardiner, J.M. Southall, Raman analysis of laser annealed amorphous carbon films, *J. Appl. Phys.* 71 (1) (1992) 521–523.
- [20] L.C. Nistor, J. Van Landuyt, V. Ralchenko, T. Kononenko, E.D. Obraztsova, V. Strel'nitsky, Direct observation of laser-induced crystallization of aC: H films, *Appl. Phys. A* 58 (2) (1994) 137–144.
- [21] F. Kreupl, R. Bruchhaus, P. Majewski, J.B. Philipp, R. Symanczyk, T. Happ, et al., Carbon Based Resistive Memory, arXiv preprint, 2009 arXiv:09014439.
- [22] A. Barreiro, F. Bornert, S.M. Avdoshenko, B. Rellinghaus, G. Cuniberti, M.H. Rummeli, et al., Understanding the catalyst free transformation of amorphous carbon into graphene by current induced annealing, *Sci. Rep.* 3 (2013).
- [23] A. Sebastian, A. Pauza, C. Rossel, R.M. Shelby, A.F. Rodriguez, H. Pozidis, et al., Resistance switching at the nanometre scale in amorphous carbon, *New J. Phys.* 13 (1) (2011) 013020.
- [24] Y. Li, A. Sinitskii, J.M. Tour, Electronic two-terminal bistable graphitic memories, *Nat. Mater.* 7 (12) (2008) 966–971.
- [25] F. Di, X. Dan, F. Tingting, C. Zhang, J. Niu, Q. He, et al., Unipolar resistive switching properties of diamondlike carbon-based RRAM devices, *Electron Device Lett. IEEE* 32 (6) (2011) 803–805.
- [26] A.V. Kolobov, P. Fons, A.I. Frenkel, A.L. Ankudinov, J. Tominaga, T. Uruga, Understanding the phase-change mechanism of rewritable optical media, *Nat. Mater.* 3 (10) (2004) 703–708.
- [27] M. Shakerzadeh, G. Loh, N. Xu, W. Chow, C. Tan, C. Lu, et al., Re ordering chaotic carbon: origins and application of textured carbon, *Adv. Mater.* 24 (30) (2012) 4112–4123.
- [28] M. Shakerzadeh, M. Samani, N. Khosravian, E.H.T. Teo, M. Bosman, B.K. Tay, Thermal conductivity of nanocrystalline carbon films studied by pulsed photothermal reflectance, *Carbon* 50 (3) (2012) 1428–1431.
- [29] M. Shakerzadeh, E.H.T. Teo, A. Sorkin, M. Bosman, B.K. Tay, H. Su, Plasma density induced formation of nanocrystals in physical vapor deposited carbon films, *Carbon* 49 (5) (2011) 1733–1744.
- [30] B.K. Tay, Z.W. Zhao, D.H.C. Chua, Review of metal oxide films deposited by filtered cathodic vacuum arc technique, *Mater. Sci. Eng. R* 52 (1 3) (2006) 1–48.
- [31] B. Efron, R. Tibshirani, Bootstrap methods for standard errors, confidence intervals, and other measures of statistical accuracy, *Stat. Sci.* (1986) 54–75.
- [32] A.C. Ferrari, J. Robertson, Interpretation of Raman spectra of disordered and amorphous carbon, *Phys. Rev. B Condens Matter* 61 (20) (2000) 14095.
- [33] J.S. Speck, J. Steinbeck, M. Dresselhaus, Microstructural studies of laser irradiated graphite surfaces, *J. Mater. Res.* 5 (05) (1990) 980–988.
- [34] J. Tersoff, Empirical interatomic potential for carbon, with applications to amorphous carbon, *Phys. Rev. Lett.* 61 (25) (1988) 2879–2882.
- [35] J. Steinbeck, G. Dresselhaus, M.S. Dresselhaus, The properties of liquid carbon, *Int. J. Thermophys.* 11 (4) (1990) 789–796.
- [36] J. Steinbeck, G. Braunstein, M. Dresselhaus, T. Venkatesan, D. Jacobson, A model for pulsed laser melting of graphite, *J. Appl. Phys.* 58 (11) (1985) 4374–4382.
- [37] T. Venkatesan, D.C. Jacobson, J.M. Gibson, B.S. Elman, G. Braunstein, M.S. Dresselhaus, et al., Measurement of thermodynamic parameters of graphite by pulsed-laser melting and ion channeling, *Phys. Rev. Lett.* 53 (4) (1984) 360–363.
- [38] J. Heremans, C.H. Olk, G.L. Eesley, J. Steinbeck, G. Dresselhaus, Observation of metallic conductivity in liquid carbon, *Phys. Rev. Lett.* 60 (5) (1988) 452–455.
- [39] D.H. Reitze, H. Ahn, M.C. Downer, Optical properties of liquid carbon measured by femtosecond spectroscopy, *Phys. Rev. B Condens Matter* 45 (6) (1992) 2677–2693.
- [40] D.H. Reitze, X. Wang, H. Ahn, M. Downer, Femtosecond laser melting of graphite, *Phys. Rev. B Condens Matter* 40 (17) (1989) 11986.
- [41] CEA. Cast3M, 2015 ed 2015, <http://www-cast3m.cea.fr/index.php>.
- [42] M. Hatano, S. Moon, M. Lee, K. Suzuki, C.P. Grigoropoulos, Excimer laser-induced temperature field in melting and resolidification of silicon thin films, *J. Appl. Phys.* 87 (1) (2000) 36–43.
- [43] B.R. Tull, J.E. Carey, E. Mazur, J.P. McDonald, S.M. Yalisove, Silicon surface morphologies after femtosecond laser irradiation, *MRS Bull.* 31 (08) (2006) 626–633.
- [44] M. Huang, F. Zhao, Y. Cheng, N. Xu, Z. Xu, Origin of Laser-Induced Near-Sub-wavelength Ripples: Interference between Surface Plasmons and Incident Laser, *ACS Nano* 3 (12) (2009) 4062–4070.
- [45] A. Miotello, R. Kelly, Critical assessment of thermal models for laser sputtering at high fluences, *Appl. Phys. Lett.* 67 (24) (1995) 3535–3537.
- [46] N. Bulgakova, A. Bulgakov, Pulsed laser ablation of solids: transition from normal vaporization to phase explosion, *Appl. Phys. A* 73 (2) (2001) 199–208.
- [47] J. Bonse, S. Baudach, J. Kruger, W. Kautek, M. Lenzner, Femtosecond laser ablation of silicon modification thresholds and morphology, *Appl. Phys. A* 74 (1) (2002) 19–25.
- [48] Z. Du, A.F. Sarofim, J.P. Longwell, C.A. Mims, Kinetic measurement and modeling of carbon oxidation, *Energy Fuels* 5 (1) (1991) 214–221.
- [49] S. Raoux, G.W. Burr, M.J. Breitwisch, C.T. Rettner, Y.-C. Chen, R.M. Shelby, et al., Phase-change random access memory: a scalable technology, *IBM J. Res. Dev.* 52 (4.5) (2008) 465–479.
- [50] H. Shin, S. Kang, J. Koo, H. Lee, J. Kim, Y. Kwon, Cohesion energetics of carbon allotropes: quantum Monte Carlo study, *J. Chem. Phys.* 140 (11) (2014).
- [51] M. Avrami, Kinetics of phase change. I general theory, *J. Chem. Phys.* 7 (12) (2004) 1103–1112.